Automatic cell counting in vivo in the larval nervous system of Drosophila

Forero, Manuel G.; Kato, Kentaro; Hidalgo, Alicia

DOI:
10.1111/j.1365-2818.2012.03608.x

Document Version
Peer reviewed version

Citation for published version (Harvard):
Forero, MG, Kato, K & Hidalgo, A 2012, 'Automatic cell counting in vivo in the larval nervous system of Drosophila', Journal of Microscopy, vol. 246, no. 2, pp. 202-212. https://doi.org/10.1111/j.1365-2818.2012.03608.x

Automatic cell counting in vivo in the larval nervous system of Drosophila

Manuel G. Forero[1,2], Kentaro Kato[1] and Alicia Hidalgo[1]*

1, Neurodevelopment Group, School of Biosciences, University of Birmingham, Birmingham B15 2TT. 2, Present address: School of Biosciences, Cardiff University

* Corresponding author: Dr Alicia Hidalgo

Contact details:

Phone: 00 44 121 4145416 Fax: 00 44 121 414 54 45 a.hidalgo@bham.ac.uk

Keywords: Fluorescence microscopy, confocal microscopy, image processing, classification, cell number, glia, *Drosophila*, larva.

ABSTRACT

Identification and counting of cells is necessary to test biological hypotheses, for instance of nervous system formation, disease, degeneration, injury and regeneration, but manual counting is time-consuming, tedious, and subject to bias. The fruit-fly Drosophila is a widely used model organism to analyse gene function, and most research is carried out in the intact animal or in whole organs, rather than in cell culture. Inferences on gene function require that cell counts are known from these sample types. Image processing and pattern recognition techniques are appropriate tools to automate cell counting. However, counting cells in *Drosophila* is a complex task: variations in immunohistochemical markers and developmental stages result in images of very different properties, rendering it challenging to identify true cells. Here, we present a technique for counting automatically larval glial cells in 3D, from confocal microscopy serial optical sections. Local outlier thresholding and domes are combined to find the cells. Shape descriptors extracted from a data set are used to characterise cells and avoid over-segmentation. Morphological operators are employed to divide cells that could otherwise be missed. The method is accurate and very fast, and treats all samples equally and objectively, rendering all data comparable across specimens. Our method is also applicable to identify cells labelled with other nuclear markers and in sections of mouse tissues.

INTRODUCTION

Image processing methods offer the opportunity to extract quantitative information from fluorescence laser scanning confocal microscopy images to address biological questions: for instance, how is cell number controlled during growth, or what leads to cells dividing in excess in cancer or dying in neurodegenerative diseases? Immunohistochemistry is used to label cell nuclei in whole specimens (e.g. in vivo) or in tissues (e.g. sections or explants), confocal microscopy to capture images in 3D and image processing methods to automatically count their number. This allows comparisons between normal specimens and specimens where genes have been mutated or modified (e.g. causing over-growth or degeneration) or in regeneration after injury (Kato *et al.*, 2011). Many specimens can be analysed, enabling statistically significant conclusions.

Here, we present a method that employs image filtering and mathematical morphology techniques aimed to identify cells to automatically count all the glial cells in the ventral nerve cord (VNC) of the larva of the fruit-fly, Drosophila. Drosophila is a very powerful model organism often used to identify gene networks, investigate gene function and model human disease and the larva is commonly used for neuroscience research. Knowledge of glial number is necessary to understand how the nervous system forms, and how altered gene functions may affect nervous system structure. For instance, glial number increases in glioma, the most abundant type of brain tumours in humans, or glial number changes upon nervous system injury and repair (Kato et al., 2011). Counting glial cells manually is extremely error prone, very time consuming, labour intensive and tedious.

We have previously developed several methods to automatically count the number of glial cells, neuronal nuclei, mitotic and apoptotic cells in Drosophila

embryos (Forero *et al.*, 2009, Forero *et al.*, 2010a, Forero *et al.*, 2010b). However, none of these methods work accurately in the Drosophila larva. This is due to the fact that each antibody marker results in images of different properties, and cell number, size, shape and density increase with developmental age (i.e. embryo, larva, adult). We have tested in larvae and adult brains our programmes developed for embryos, and they do not perform accurately. In particular, DeadEasy MitoGlia (Forero et al., 2010a), which was developed to count cells labelled with Repo or p-Histone-H3, is not robust in post-embryonic tissues. DeadEasy MitoGlia employs a global threshold to binarise each image, which produced good results in embryos given high signal intensity and low attenuation through the stack. However, in larval tissues, this method produced artefacts. Thus, using only one method compromises accuracy to the extent of rendering results uninformative. For this reason, developing different methods was paramount for accuracy.

Image processing methods overcome the technical difficulties associated with manual counting by treating all samples more objectively and consistently than humans can, thus minimising error. Automatic counting is also less labour intensive and avoids tedium. Thus it was necessary to develop an automatic method that would be fast and accurate for the Drosophila larva.

Unfortunately, identifying and counting cells are also challenging for image processing. Difficulties arise from the properties of the equipment, labelling quality, irregular shape and size of cells, and cell clustering (Dima *et al.*, 2002, Meijering & van Cappellen, 2007, Peng, 2008). For the latter, each cell can be identified from an initial seed, but methods need to be applied to prevent over-segmentation (i.e. the marking of one cell with more than one seed), such as developing a seeding procedure during sample preparation (Yu *et al.*, 2009), or clustering methods or

morphological filters (Vincent, 1993, Clocksin, 2003, Svensson, 2007, Yu *et al.*, 2009). Watershed based algorithms are frequently used for cell segmentation (Vincent & Soille, 1991, Lockett & Herman, 1994, Malpica *et al.*, 1997). Cells are also treated like fuzzy objects and seeds detected as the peaks of the fuzzy distance transforms (Svensson, 2007), employing topographical distance functions (Hodneland *et al.*, 2009), or level set functions (Yu et al., 2009). Gradient flow tracking is an alternative approach (Li *et al.*, 2007, Li *et al.*, 2008). Wählby et al. (Wählby *et al.*, 2002, Wählby, 2003, Wählby *et al.*, 2004) developed a technique that combines morphological filtering, the gradient of the images and the data's shape to segment cells in 2D and 3D images. Other authors used a 3D watershed algorithm to separate cells and then employed shape descriptors to break watershed surfaces, using scores for each nucleus, and measuring how well the nuclei fit a statistical model (Lin *et al.*, 2003). Morphological descriptors can also be extracted from training data to generate features which are then used for classification of nuclei (Jeong *et al.*, 2009). Overlapping nuclei are segmented using an intensity gradient transform and watershed algorithm to separate them. These procedures can yield good results in 2D and 3D. Unfortunately, good results were not consistently obtained in Drosophila larval samples, most particularly if image resolution was low, stacks consisted of anisotropic voxels or cell density was high with many cells abutting one another.

Most 3D image processing techniques aiming to improve segmentation make a correction for fluorescence intensity, which decays due to photo-bleaching. However, these methods do not produce consistently good results, particularly if images have background signal revealing the tissue. Furthermore, working with 3D images presents a further problem. Whilst it is usually ideal to acquire stacks

composed of cubic voxels, larval ventral nerve cords are on average 120 micrometers thick: acquiring continuous images at this resolution is not practical, since it would take a long time and fluorescence would bleach. A solution is to acquire stacks of images with anisotropic voxels, keeping a high x-y resolution to visualise nuclei and increasing the step between images while still seeing the same nuclei in several slices.

Here, as for our other methods (Forero et al., 2009, Forero et al., 2010a, Forero et al., 2010b), we used 2D techniques for image processing and 3D after the images had been binarised. This yielded good results from stacks of images with anisotropic voxels. The method was applied to images captured from different focal planes that constitute a complete stack of the microscopy field where the region of interest is present. Within a given set of conservative parameters, automatic quantification might lead to slight underscoring. Nevertheless, the method accepted or rejected cells using the same criteria, eliminating subjectivity. Given its simplicity, the method is very fast without losing accuracy. We compare the effectiveness of this algorithm against the results obtained using CellSegmentation3D developed by Li *et al*. (2007). We have recently used this method successfully to investigate repair after injury in the Drosophila larva (Kato et al., 2011).

METHODS

Experimental procedures and image acquisition

Drosophila melanogaster fruitflies were used of the following genotypes: (1) for controls: *yw*; (2) for over-expression: *repoGAL4* flies crossed to *UASact-htl* flies, and (3) *alrmGAL4* flies (gift of Marc Freeman) crossed to *UAShistoneYFP* flies.

Larval ventral nerve cords were dissected, fixed and labelled with pan-glial nuclear marker mouse anti-Repo antibodies (DSHB, at 1:250 dilution) (Figure 1), using standard immunohistochemistry procedures, except that fixation was in PEM buffer and 0.3%Triton in PBS was used as described in Kato et al ((Kato *et al.*, 2009). Antibody-labelled cells were detected with anti-mouse or anti-Guinea pig secondary antibodies directly conjugated to Alexa-Fluor 488 (at 1:250). Other antibodies used in this study were: rabbit anti-GFP 1:1000 (Molecular Probes); Guinea pig anti-HB9 1:2500 (gift of H. Broihier); rabbit anti-pHistone-H3 1:250 (Upstate Biotechnolgy); and anti-Guinea pig or anti-rabbit Alexa Fluor 488 or 647-conjugated secondary antibodies (Molecular Probes). DAPI (1µg/ml, SIGMA) was used to stain nuclei in cryosections of rat spinal cords (thickness of 10µm, gift of A. Logan).

Specimens were mounted in 80% glycerol in PBS. Specimens were scanned with a laser scanning Bio-Rad Radiance 2000 MP confocal microscope or with a Leica SP2-AOBS confocal microscope. Image acquisition was carried out using a 40X magnification oil immersion lens and no averaging, with the following settings: (1) for BioRad: image size 512 X 512 pixels, and pixels size 0,5665 X 0,5665 microns, step 0.96 microns; (2) for Leica: image size 512x512 pixels, pixel size of 0.7332 X 0.7332 microns, step 1.2 microns. The mathematical algorithms to quantify glial cell nuclei computationally were developed using Java, as plug-ins for the publicly availably ImageJ software. The software was developed in a Pentium 4, 3 GHz computer with 1.5 GB RAM running under Ubuntu Linux. The method will become publicly available through our lab webpage (www.biosciences-labs.bham.ac.uk/hidalgo).

Image processing: automatic counting of all glial cells

Repo labels the nuclei of all Drosophila glial cells except the midline glia (Figure 1) and the image processing method we developed here was tuned specifically to count glial cells in larvae, which vary more in size and shape, and are more numerous than embryonic glia. The algorithm developed proceeds in several steps as follows (Figure 2).

Cells labelled with Repo are characterised by high signal intensity and low background. Since there are numerous glial cells in the larval VNC, Repo positive cells can form tight clusters, making it difficult to separate and identify cells (Figure 1B,D). Other challenges were: 1) cell shape was not consistently spherical. 2) Repo positive nuclei could vary considerably in size: immediately after cell division, pairs of small Repo positive cells were in contact and needed to be separated, and some glial types were considerably larger due to endoreplication. 3) The edges of the larval nerve cord could fluoresce. This non-specific signal was made up of particles, which might be recognised as candidate objects by the programme, thus they had to be rejected manually. This was done by drawing a region of interest (ROI) tightly along, and excluding, the edge of the nerve cord. Samples with high non-specific background or strong staining along the edge were discarded.

To identify the cells of interest in a stack of images, the first step is a noise reduction filtering. Given that image acquisition is based on photon detection, the major source of error follows a Poisson distribution. Several noise reduction techniques based, for instance, on wavelets can be employed, but they are time consuming and their use becomes prohibitive when it is necessary to work with large numbers of images and stacks. Therefore, a median filter was employed (Figure 2

and Figure 3B). This provided good results, reducing the noise and the significant intensity heterogeneity typical of confocal images without smoothing the borders and valleys between the cells.

After median filtering, segmentation was carried out. Because cell borders are fuzzy, a thresholding technique was preferred over edge segmentation. However, due to considerable variation in signal intensity, a global threshold did not produce good segmentation. If the threshold was high, some areas containing cells could be missed, and if it was low, large areas of background could be selected as belonging to foreground. Furthermore, Repo labelled cells did not have uniform signal intensity, and there were regions of high intensity separated by others of low intensity. Therefore, if a global threshold were employed, a cell could be split into several parts. For this reason, a local thresholding method was employed instead (Figure 3C). Rather than using one threshold per image, a threshold was found for each pixel according to the intensity of the surrounding pixels. A circular window *W*, with diameter greater than the maximum diameter of a cell, was centered in each pixel located in (*x,y*). If the difference between the central pixel and the median of the pixels inside *W*, was higher than a predefined threshold *t*, the pixel was assigned a value of 1. Alternatively, it was given a value of zero, that is:

$$r(x,y) = \begin{cases} 1 & \text{if} \quad \underset{i,j \in W}{\text{med}} q(i,j) - q(x,y) > t \\ 0 & \text{in other cases} \end{cases}$$

where $q(x,y)$ and $r(x,y)$ are the input and the resulting images, respectively. t was chosen according to the typical minimal variation in intensity between the cells and the background. A value of $t=30$ was found empirically.

In parallel to thresholding, a morphological opening operation with a circular

structuring element of radius 1.5 was developed to eliminate very small particles and render signal intensity within each cell more uniform, which was important to reduce the number of domes or seeds found per cell (Figure 3D). The result of thresholding was then employed as a mask to only select the zones were cells appeared. This was done by selecting the minimum value for each pixel (Figure 2 and Figure 3E):

$$t(x,y)=\min[r(x,y),s(x,y)]$$

where $t(x,y)$ is the resulting image and, $r(x,y)$ and $s(x,y)$ the input images.

Once the region where the cells were contained was identified, it was necessary to find a seed for each cell (Figure 3F). A seed is a small part of a cell, not connected to another cell, that can be used to mark it. Seeds were found in the following way. An image can be viewed as an orographic system, where labelled cells are like peaks or domes separated by dark valleys, and whose height is determined by the intensity of the pixels (Vincent, 1993). To identify each cell, a dome or regional maxima higher that a height *h* had to be found (Figure 2). Given that the signal-to-noise ratio (SNR) of the Repo-labelled images is low, noise often produced domes in the background. However, domes due to noise were rejected in the previous thresholding step, as only the areas where cells appeared were taken and separated from the background. To find the domes, a 2D regional maxima detection was performed, and a h-dome operator (Vincent, 1993) was applied to extract and mark the cells. The choice of *h* is generally not critical since a range of values can provide good results (Vincent, 1993). In order to determine *h*, we observed the profile of the cells in images with very poor contrast with respect to the background. The minimum difference between the maximum grey level of the nuclei and the surrounding pixels was approximately between 3 and 8. As a test, we ran the

program using values of *h* between 2 and 10 (Table 1). As a result, *h*=5 was selected empirically as a good value for marking all cells.

Subsequently, the h-dome images were binarised by assigning a value of 1 to all the pixels of intensity higher or equal to 1 (Vincent, 1993), that is,

$$r(x,y) = \begin{cases} 1 & h(x,y) > 0 \\ 0 & \text{in other cases} \end{cases}$$

where h(x,y) and *r*(*x,y*) are the input and the resulting images respectively, resulting in good identification of cells (Figure 3G).

Due to variation in signal intensity, several seeds could potentially be found within one cell. To avoid this, the gradient between seeds was previously used as a means to determine if two seeds belong to the same cell (Wählby, 2003, Wählby et al., 2004). However, we found that this procedure did not provide good results with our samples. On the one hand, due to signal fuzziness and low resolution, there was not always a notable change in signal intensity at the borders between two cells, and seeds belonging to different cells were taken as one. On the other hand, due to high variation in signal intensity inside some cells, multiple seeds were still detected per cell. Thus, the morphological opening step mentioned above (Figure 2) was also introduced to reduce the number of seeds per cell (most particularly in cells with high heterogeneity in signal intensity).

Glial cells are mainly recognized from their shape. Information on cell shape can be employed to determine if two or more seeds belong to only one cell. Therefore, in parallel, we identified cells by their shape (Figure 2). A good approximation to cell shape was provided from the images resulting from the thresholding step (Figure 3G), particularly from isolated cells or cells that could be easily separated using a 2D watershed procedure (Figures 2 and Figure 3H). Cells identified by their shape were retained, while other particles were removed (Figure

3I). Repo labelled cells had an ovoid or elliptical shape that could become almost circular. In order to identify the best characteristics than can be employed to describe the cells, a statistical analysis was developed following the steps previously employed by Forero et al (2006). For a robust identification, cell representation must ideally be translation, rotation and scale invariant. Compactness, eccentricity, Hu's moments and Fourier descriptors are compliant with this requirement. Fourier descriptors were not considered for the study given the tiny size of cells, which rendered cells' contours very sensitive to noise. Therefore, only Hu's moments, compactness and eccentricity were considered.

Compactness *C* is defined as:

$$C = \frac{P^2}{A}$$

where *A* and *P* represent the area and perimeter of the object, respectively. The moment invariants were obtained from the binarised image of each cell; pixels inside the boundary contours were assigned a value of 1 and pixels outside a value of 0. The central moments were given by:

$$\mu_{rs} = \sum_{xy} (x - \bar{x})^r (y - \bar{y})^s f(x,y), \text{ for } r + s = 2,3,...,\infty .$$

where *f*(*x*,*y*) represents a binary image, *p* and *q* are non-negative integers and $\bar{x}$, $\bar{y}$ is the centroid. From the central moments Hu (Hu, 1962) defined seven rotation, scale and translation invariant moments of second and third order. As cells have a symmetrical shape, the third and higher odd order moments are close to zero. Therefore, the first three-order Hu's moment ϕ_3 is sufficient to recognize symmetrical objects. ϕ_3 is given by:

$$\phi_3 = \left(\eta_{30} - 3\eta_{21}\right)^2 + \left(3\eta_{21} - \eta_{03}\right)^2$$

where $\eta_{rs} = \frac{\mu_{rs}}{\mu_{00}^{\gamma}}$ and $\gamma = \frac{r+s}{2} + 1$, $r + s = 2,3,...,\infty$.

Assuming that each descriptor follows a Gaussian distribution, we found that the best descriptor to discriminate circular cells was compactness, as it had the lowest standard deviation. However, when two or more cells were close together, their added shape could also have high compactness, even if not as high as that of a circular object. In order to distinguish circular cells from clusters of several cells, a threshold was defined. To find the minimum compactness, a set of 182 samples of shapes from clusters of two or more cells were analysed (Figure 4 and Table 2). The value of maximum compactness *C*=0.85 was found to be the minimum threshold for circular cells.

Many cells were ovoidal, with lower compactness. Symmetry measured by ϕ_3 enabled to distinguish elliptical cells from other objects with similar compactness but lower symmetry. Given that there is no rule to define when an object is ovoid or symmetric or not, the threshold values for compactness and symmetry for ovoidal cells were established empirically. Thus, an object was considered a cell if:

$0.85 \leq C \leq 1$

or:

$0.7 \leq C$ and $\phi_3 \leq 0.00009$

and remaining particles were removed from each image. The advantage of this procedure is that for a stack of images, virtually every cell was isolated as circular or ovoidal in at least one image. This allowed combining several seeds per cell into one, thus solving the problem of identifying multiple seeds per cell (Figure 3I and

Figure 5C).

Adjacent cells could overlap, from one image to another, being later connected, due to the superposition of their shapes. Therefore, to separate individual cells, once the circular and elliptical shapes were selected, all particles in the stack were eroded (Figure 3J and Figure 5D). This reduced the area of the objects and increased the distance between them, thus eliminating overlaps.

In some cases there was no significant change in intensity between abutting cells, and consequently one dome could correspond to only one seed for two or more cells (Figure 5E). Thus, despite the fact that cells had been separated in the shape analysis step (Figure 3I), if they were only identified by one seed, they were reconnected in the OR operation during the combination of seeds procedure (Figure 5F). As a consequence, these cells might again reappear connected. To solve this problem, it was necessary to delete the part of the dome that lies between the circles (Figure 2 Object separation and Figure 6). The first step consisted of an AND operation in order to find the intersection points between the cells' shapes and the seed (Figure 6C). The result of the intersection was used to find the shape of the dome with a 2D region growing reconstruction starting from the intersection pixels (Figure 6D). Then, the region between the circles to be eliminated was found by subtracting the intersection pixels from the dome (Figure 6E). The region was then eliminated by subtracting it from the image resulting of the OR procedure (Figures 5F and Figure 6F), obtaining the separated seeds (Figures 2 and Figure 6G).

The objects in the stack were labelled in 3D using 18-connectivity, allowing to identify each object through the different slices and cell shape was recovered by applying a 3D region growing starting from each labelled object as seed, and the

stack resulting of the local thresholding as mask (Figure 2 and Figure 3N). Finally, Repo positive cells were identified amongst the candidate objects. The volume of each object was obtained by multiplying the number of voxels in the object by the volume of each voxel. It was found empirically that Repo cells have a volume *V* of $30.8<V<1232.34\ mm^3$, *i.e.* a 3.5x variation in size (Figure 3O), and remaining objects were rejected.

Automatic counting of manually selected cells for restricted cell-type counting

It may also be desirable to know the number of cells of a given type. This can be carried out marking the cells manually, aided of the "Cell counter" ImageJ macro. However, with this method the marker is only a small dot, which renders it difficult to see which cells have been marked. We developed a simple method that enables the user to mark the whole cell in 2D and 3D, and count them automatically (Figure 7). The first step consisted of median filtering to reduce noise. Then, each cell throughout the stack was selected using the computer mouse. Once a voxel of a cell was selected, a 3D region growing procedure was employed in order to mark the cell through the stack. That is, the selected voxel was employed as a seed and compared with neighbouring voxels. The region grew by adding voxels that are similar in intensity. The added pixels were employed as new seeds and the process was repeated until no more voxels were added to the region. In this way, a voxel was added to the region if the difference between the neighbour voxel and the mean $\hat{\mu}$ of the voxels already included in the region was lower than a threshold q_{dif} specified by the user, that is:

$$\left|q(x,y,z) - \hat{\mu}\right| < q_{dif}$$

and $q(x,y,z) > q_{\min}$, where $q_{\min}$ is the minimum grey level that can have a voxel belonging to the region. Once all cells had been selected, they were labelled and counted automatically with the method described above (Figure 7).

RESULTS

The image processing method we have developed – and which name DeadEasy Larval Glia - identifies cells, and produces a stack of images with the same number of images as the original raw stack, where the identified cells are reproduced in corresponding locations. To validate the technique, we generated a merged stack of images, combining the original raw stack with the processed stack of identified objects (as previously done for similar methods (Forero et al., 2010b), Figure 8A). In the raw and processed stacks cells are labelled in different colours and in the merged stack co-localising cells appear in a different colour. For instance in Figure 8A, cells in the raw stack appear green; cells in the processed stack, magenta; and merged cells present in both stacks appear white. We analysed the merged stack by scrutinising each cell one by one. First, we looked at their colour in 3D (i.e. through multiple optical sections) as this reveals the likelihood of being correctly identified. Subsequently, we verified the presence or absence of the cell in the raw and processed stacks. Every cell was scrutinised one by one to determine if: (1) it was a true Repo labelled cell, (2) it was instead an object present in the processed stack and therefore detected by the programme but which did not correspond to a real cell (false positive), (3) or a cell present in the original raw stack but missed by the programme (false negative). The method performed accurately in the quantification of cells (Table 3). The counting was conservative, in that the error given by false

positives was negligible, whilst some cells were missed. The small percentage of false negatives is however not a concern, since the same criteria is used for all images and samples. Tissue depth did not increase error, at least when using anti-Repo, since false positives and false negatives were distributed uniformly throughout the stack. Instead, error correlated with object size and pixel intensity. There is no bias during the practical application of the technique.

To verify how reliably the method performed, we compared it with manual counting by one person done three times, or by three different people (Table 3). DeadEasy Larval Glia always produced the same count irrespectively of how many times it was run over the same sample (i.e. standard deviation is 0). Manual counting was carried out marking the cells manually and then either using “Cell Counter” or our own macro as described above. When one person counted cells three times, the number of cells counted per sample was different each time (i.e. standard deviation ≠0, see Table 3). When three different people counted cells in the same set of samples, their counts differed even further (Table 3). This demonstrates that the method developed here is more reliable than human counting. DeadEasy software is also fast. It takes approximately 50 seconds to count around 500 glial cells in a stack of approximately 146 images. Human counting can take up to13 minutes for every 100 cells.

We tested further the performance of our method by comparing it with CellSegmentation3D (using the values suggested by the authors), developed by Li *et al*. (2007), which is publicly available. Our software performed better at separating clustered cells, while keeping low the number of false positives (Table 4). In order to reduce the number of false negatives obtained with CellSegmentation3D we reduced the minimum size of regions or particles to be accepted as cells from 50 (default

value) to 15. The number of false negatives was reduced from 12.77 to 8.02, but the number of false positives increased from 0 to 0.73%. We found that in addition to missing more cells, CellSegmentation3D was in general less successful than DeadEasy at detecting joined cells (Figure 9). Thus, DeadEasy performed better.

Our method differs from and surpasses our previously developed method DeadEasy MitoGlia, which could also identify Repo-labelled cells, although only in the Drosophila embryo (Forero et al., 2010a). DeadEasy MitoGlia used a global threshold to binarise each image, which produced good results in embryos, in which signal intensity was very high and there was little fluorescence attenuation through the stack. However, in larvae, this thresholding method produced artefacts and it was not robust to noise. This was likely due to a combination of larval tissues being thicker, with higher cell density, with signal variation, ten times increase in cell size, and change in cell shape. For DeadEasy Larval Glia, we took advantage of cell shape, improving the identification of abutting cells whilst avoiding over-segmentation.

To put to the test the application of this method to address biological questions, we counted the number of glial cells in normal larvae, and compared it with counts in larvae in which the FGFR receptor homologue Heartless (Htl) had been constitutively activated in glia (using *repoGAL4* and *UAS-activated-Heartless*). We show that in normal larvae there are around 500 glial cells and upon activation of Htl up to 2,500 glia per abdominal VNC (Figure 8B). Thus, our method enables the analysis of cell number in many specimens of many different genotypes to reach statistically significant conclusions on the effects of altering gene function.

The programme can be optimised to work on other sample types by changing

the parameters as indicated in Figure 8C and Table 5. As a starting point, we tested whether our method – without any modifications - could count cells labelled with other markers, or in other sample types. In Drosophila larvae, DeadEasy Larval Glia counted accurately sparsely distributed nuclei labelled with Histone-YFP (seen here in glia, in larvae of genotype *alrmGAL4>mCD8GFP* Figure 10A). The programme did not identify accurately cells labelled with BrdU (not shown), as this marker frequently resulted in large clusters of cells where their boundaries merged. The method was quite accurate identifying neuronal nuclei labelled with HB9, although there were some false negatives (Fgure 10B). The method identified accurately all dividing cells labelled with phospho-Histone-H3 (Figure 10C). We also tested whether the programme could be used to count cells in mammalian tissues. For this, we tested sections of the mouse spinal cord labelled with nuclear markers. DeadEasy identified very accurately mouse white matter nuclei labelled with Sytox Green (not shown), and it also identified well white matter nuclei labelled with DAPI (Figure 10D), although false negatives were found. Users ought to validate the use of the programme in samples different from those used for its development, and minimise error changing the parameters as indicated above (Table 5). Our programme is accurate at identifying Drosophila larval nuclei labelled with a range of markers and can also be used on mammalian samples.

CONCLUSION

To conclude, we have developed an automatic technique to count Repo labelled glia cells using images from the Drosophila larval VNC. This method has been successfully employed to investigate repair after injury in Drosophila (Kato et al.,

2011). Counting such cells manually is almost impossible, it is extremely error prone as well as tedious and labour intensive. Our image processing technique is very accurate and reproducible when counting Drosophila larval cells visualised with the same label (Repo) as employed in its development. The programme is also accurate at identifying cells labelled with other nuclear markers in Drosophila larvae, and it performs well in sections of mammalian tissues. The programme will become publicly available as an ImageJ plug-in (including source code) through the authors' website, and users will be able to modify the parameters and validate the programme for other applications.

ACKNOWLEDGMENTS

This work was funded by The Wellcome Trust Equipment Grant 073228 and BBSRC Project grant BB/H002278/1 to A.H and EU International Incoming Fellowship GRR 039842 to K.K.

REFERENCES

Clocksin, W. F. (2003) Automatic segmentation of overlapping nuclei with high background variation using robust estimation and flexible contour models. In: *Proc. 12th Int. Conf. Image Anal Process.*

Dima, A., Scholz, M. & Obermayer, K. (2002) Automatic segmentation and skeletonization of neurons from confocal microscopy images based on the 3-D wavelet transform. *IEEE T Image Process,* **11,** 790-801.

Forero, M. G., Cristobal, G. & Desco, M. (2006) Automatic identification of

Mycobacterium tuberculosis by Gaussian mixture models. *J. Microsc.,* **223,** 120-132.

Forero, M. G., Learte, A. R., Cartwright, S. & Hidalgo, A. (2010a) DeadEasy Mito-Glia: automatic counting of mitotic cells and glial cells in Drosophila. *PLoS One,* **5,** e10557.

Forero, M. G., Pennack, J. A. & Hidalgo, A. (2010b) DeadEasy neurons: automatic counting of HB9 neuronal nuclei in Drosophila. *Cytom. A,* **77,** 371-378.

Forero, M. G., Pennack, J. A., Learte, A. R. & Hidalgo, A. (2009) DeadEasy caspase: automatic counting of apoptotic cells in Drosophila. *PLoS One,* **4,** e5441.

Hodneland, E., Tai, X.-C. & Gerde, H.-H. (2009) Four-Color Theorem and Level Set Methods for Watershed Segmentation. *Int J Comput Vision,* **82,** 264-283.

Hu, M. (1962) Visual pattern recognition by moment's invariant. *IRE T. Inform. Theor.,* **8,** 179-187.

Jeong, M. R., Ko, B. C. & Nam, J. Y. (2009) Overlapping nuclei segmentation based on Bayesian networks and stepwise merging strategy. *J. Microsc.,* **235,** 188-198.

Kato, K., Awasaki, T. & Ito, K. (2009) Neuronal programmed cell death induces glial cell division in the adult Drosophila brain. *Development,* **136,** 51-59.

Kato, K., Forero, M. G., Fenton, J. C. & Hidalgo, A. (2011) The glial regenerative response to central nervous system injury is enabled by Pros-Notch and Pros-NFkB feedback. *PLoS Biol.,* **9,** e1001133.

Li, G., Liu, T., Nie, J., Guo, L., Chen, J., Zhu, J., Xia, W., Mara, A., Holley, S. & Wong, S. T. C. (2008) Segmentation of touching cell nuclei using gradient flow tracking. *J. Microsc.,* **231,** 47-58.

Li, G., Liu, T., Tarokh, A., Nie, J., Guo, L., Mara, A., Holley, S. & Wong, S. (2007) 3D

cell nuclei segmentation based on gradient flow tracking. *BMC Cell Biol.,* **8,** 40.

Lin, G., Adiga, U., Olson, K., Guzowski, J. F., Barnes, C. A. & Roysam, B. (2003) A hybrid 3D watershed algorithm incorporating gradient cues and object models for automatic segmentation of nuclei in confocal image stacks. *Cytom. A,* **56A,** 23-36.

Lockett, S. J. & Herman, B. (1994) Automatic detection of clustered, fluorescent-stained nuclei by digital image-based cytometry. *Cytometry,* **17,** 1-12.

Malpica, N., de Solórzano, C. O., Vaquero, J. J., Santos, A., Vallcorba, I., Garcia-Sagredo, J. M. & del Pozo, F. (1997) Applying Watershed Algorithms to the Segmentation of Clustered Nuclei. *Cytometry,* **28,** 289-297.

Meijering, E. & van Cappellen, G. (2007) Imaging Cellular and Molecular Biological Function. (eds. S. L. Shorte & F. Frischknecht). Springer, Berlin.

Peng, H. (2008) Bioimage informatics: a new area of engineering biology. *Bioinformatics,* **24,** 1827-1836.

Svensson, S. (2007) A decomposition scheme for 3D fuzzy objects based on fuzzy distance information. *Pattern Recogn Lett,* **28,** 224-232.

Vincent, L. (1993) Morphological Grayscale Reconstruction in Image Analysis: Applications and Efficient Algorithms. *IEEE T Image Process,* **2,** 176-201.

Vincent, L. & Soille, P. (1991) Watersheds in digital spaces: an efficient algorithm based on immersion simulations. *IEEE T Pattern Anal,* **13,** 583 - 598.

Wählby, C. (2003) Algorithms for applied digital image cytometry. Upsala University.

Wählby, C., Lindblad, J., Vondrus, M., Bengtsson, E. & Björkesten, L. (2002) Algorithms for cytoplasm segmentation of fluorescence labelled cells. In: *Anal Cell Pathol.*

Wählby, C., Sintorn, I. M., Erlandsson, F., Borgefors, G. & Bengtsson, E. (2004) Combining intensity, edge and shape information for 2D and 3D segmentation of cell nuclei in tissue sections. *J Microsc,* **215,** 67-76.

Yu, W., Lee, H. K., Hariharan, S., Bu, W. & Ahmed, S. (2009) Quantitative neurite outgrowth measurement based on image segmentation with topological dependence. *Cytom. A,* **75A,** 289-297.

FIGURE LEGENDS

Figure 1 The glia of the larval VNC. (A) Drawing illustrating a Drosophila larva, and in grey the ventral nerve cord (VNC), brain and optic lobes. (B-D) Confocal microscopy images from the abdominal portion of the VNC, labelled with the nuclear glial marker anti-Repo. (C) Single optical section; (B,D) 3D rendering of an entire stack of images throughout the thickness of the VNC; (B) transverse view; (D) longitudinal horizontal view.

Figure 2 Block diagram of the method developed to count Repo labelled cells in the larval VNC of Drosophila.

Figure 3 Images resulting from each processing step to identify Repo labelled cells. Each step corresponds to one step in the diagram in Figure 2.

Figure 4 Sample of data set of clustered cells.

Figure 5 Problems encountered when only one seed is found for two or more cells. Each step corresponds to the steps on the right in Figure 2, below "Morphological opening", and between the "Thresholding step" and the "OR" step.

Figure 6 Images resulting form the process to solve the problem shown in Figure 5. These steps are included within the "Object separation" step on the left of Figure 2, between "Binarisation" and "Subtraction".

Figure 7 Automatic counting of manually selected glia. This illustrates how a subset of cells of interest can be selected manually, and these cells can subsequently be counted automatically. n

Figure 8 Validation and biological application. (A) The programme is validated as follows: in the stack of raw images cells are labelled with Repo in green, in the stack of processed images the identified cells are labelled in magenta and a merged stack is created where the correctly identified cells appear white, false negatives appear green and false positives appear magenta. Not all cells that are present in both stacks appear white in every image (i.e. optical section), as cells have 3D shape and colocalisation may be more pronounced in different optical sections. Each cell was analysed one-by-one in the merged stack and compared with the raw and processed stacks, to quantify the false positives and false negatives. (B) Application of the method to address biological questions. Here, we show the number of glial cells in the abdominal VNC of normal larvae (wild-type, n=6) and in larva over-expressing the activated form of the FGFR homologue Htl in

glia (glia>act-Htl, n=3 using the driver repoGAL4, genotype UAS-act-Htl/+; repoGAL4/+). Expression of activated-Htl results in a dramatic increase in glial number. (C) An interactive window is provided for users to modify the parameters and adapt the programme to other sample types following Table 3.

Figure 9 Cell separation by CellSegemntation 3D compared to DeadEasy. Examples are given here of how the two methods perform at separating cells in three different samples. 34min, 64min and 104min indicate tested settings for CellSegmentation 3D.

Figure 10 How well DeadEasy Larval Glia performs on other sample types. (A-D) Left columns: raw images of cells labelled with a range of markers; centre: processed images with cells as identified by the programme; right: merged images to show the method's performance. (A-C) The programme identifies well Drosophila larval cells labelled with: (A) anti-GFP in an *alrmGAL4/UASmCD8GFP* genetic background; (B) the neuronal marker anti-HB9, but it is less accurate as there can be false negatives (arrows); (C) anti-phospho-Histone-H3, very accurately. (D) Section of a mouse spinal cord, showing nuclei labelled with DAPI in the white matter. The programme performs well, although there are false negatives. These could be corrected by optimising the parameters as in Table 3 followed by validation.

Table 1. Variation in the number of counted cells for different values of h.

Table 2. Statistical results of the analysis of compactness of clusters of cells.

Table 3. Validation.

Table 4. Compared performance of DeadEasy versus CellSegmentation 3D.

Table 5. Parameters that can be altered and their effects.

Figure 1 The glia of the larval VNC

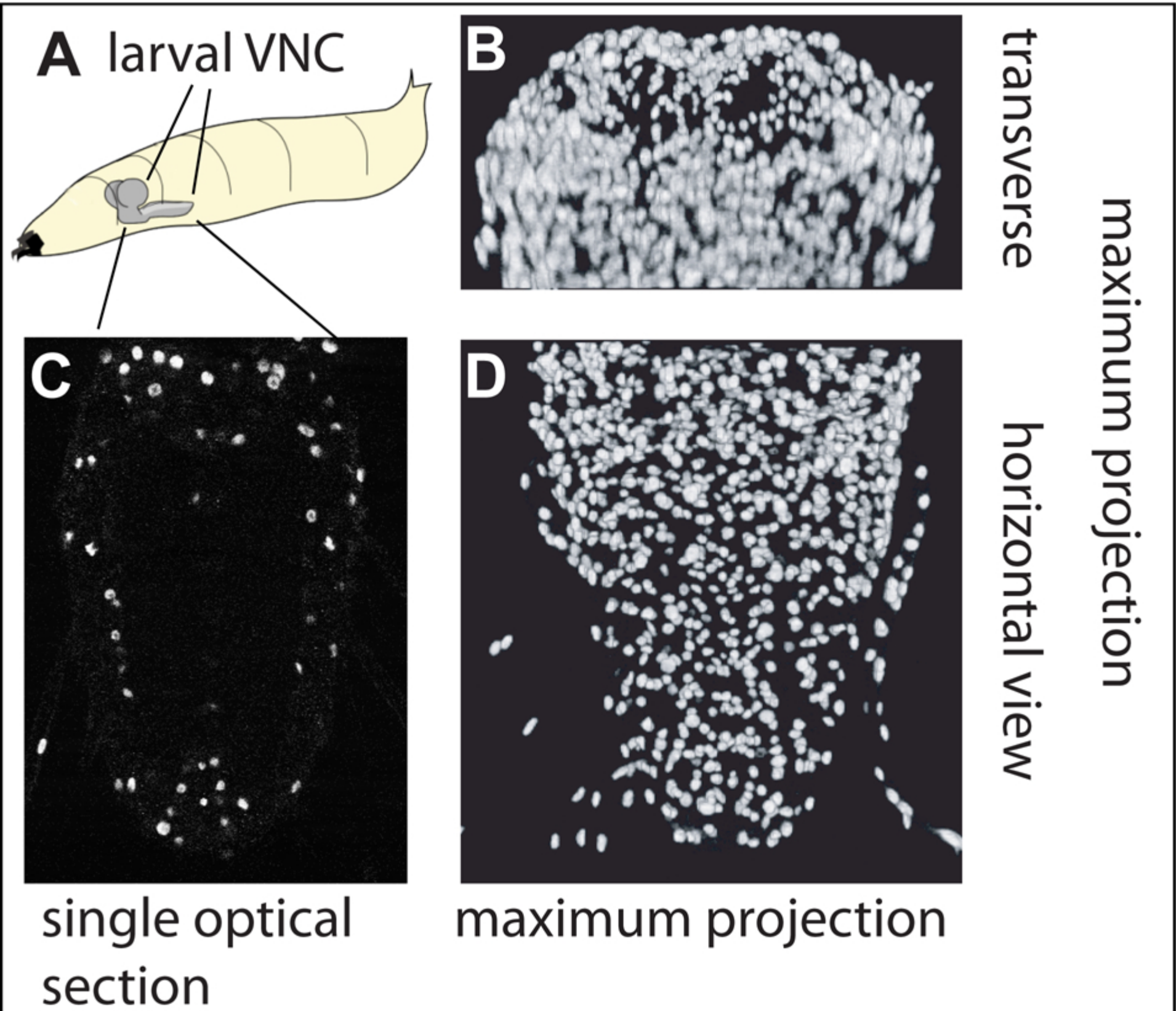

Figure 2 Block diagram of the method developed to count Repo labelled cells in the larval ventral nerve cord of Drosophila.

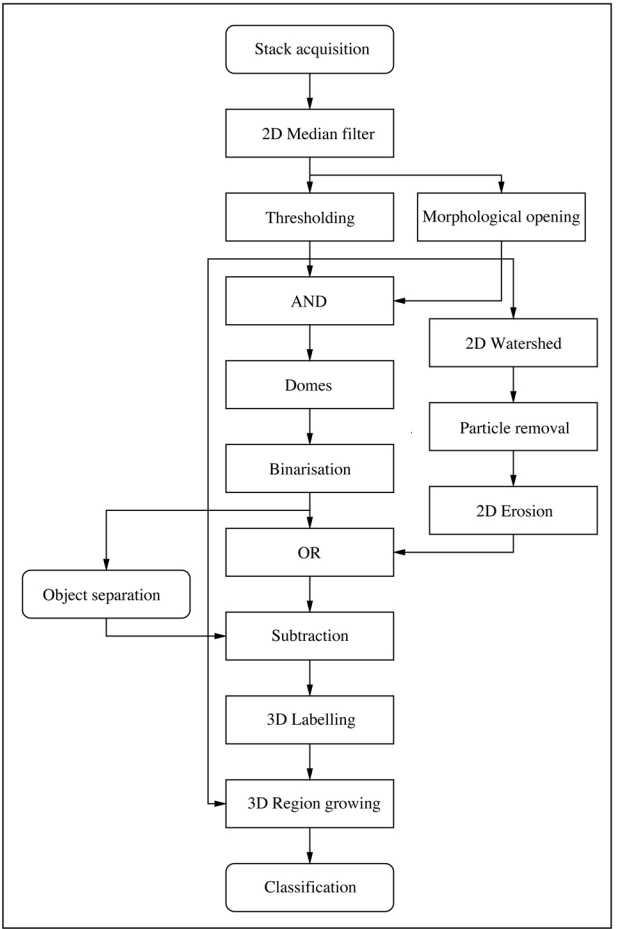

Figure 3
Images resulting from each mage processing step to identify Repo labelled cells

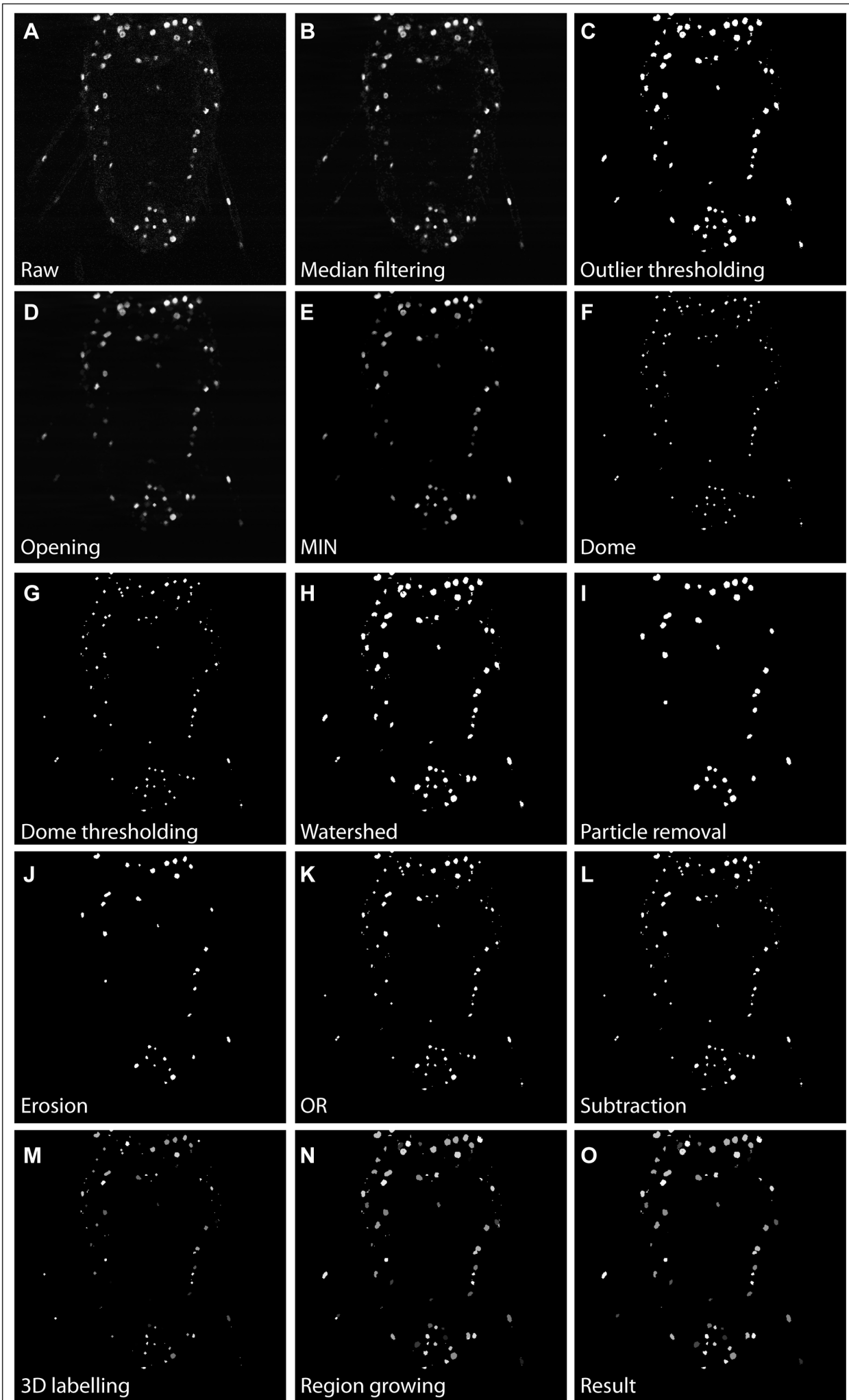

Figure 4 Sample of data set of clustered cells

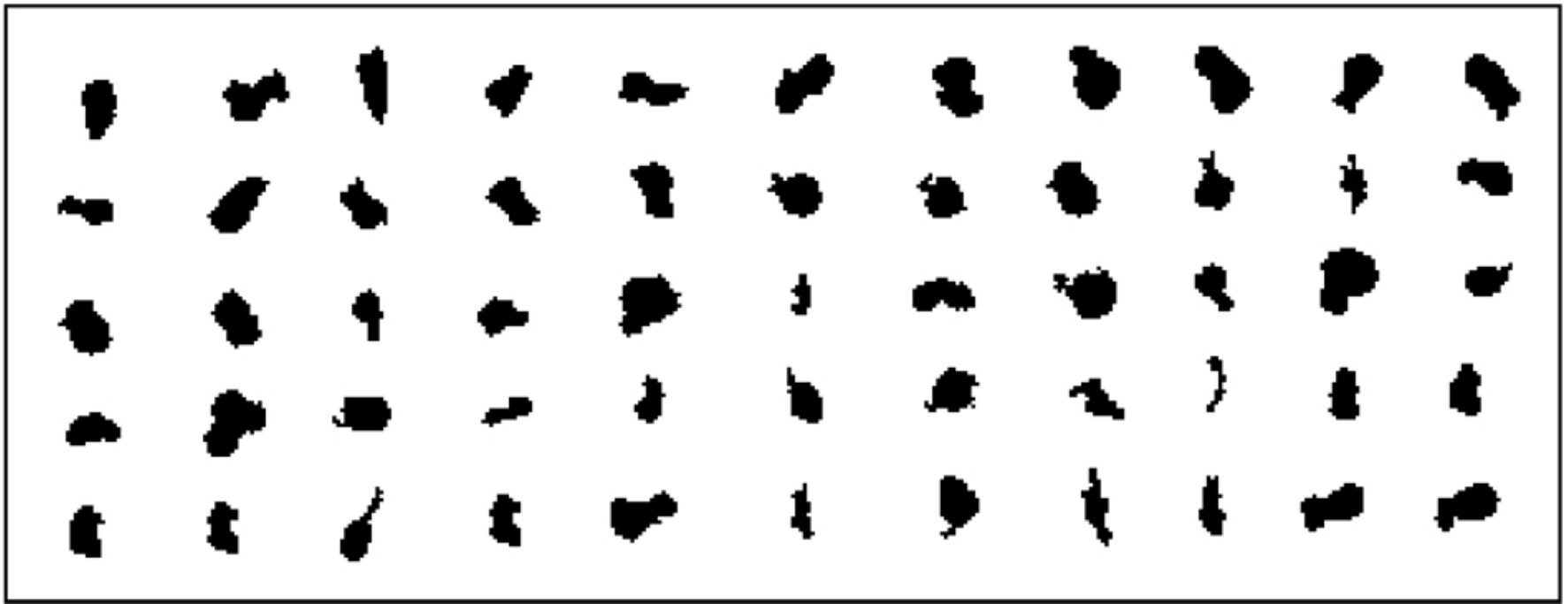

Figure 5 Problem encountered when only one seed is found for two or more cells

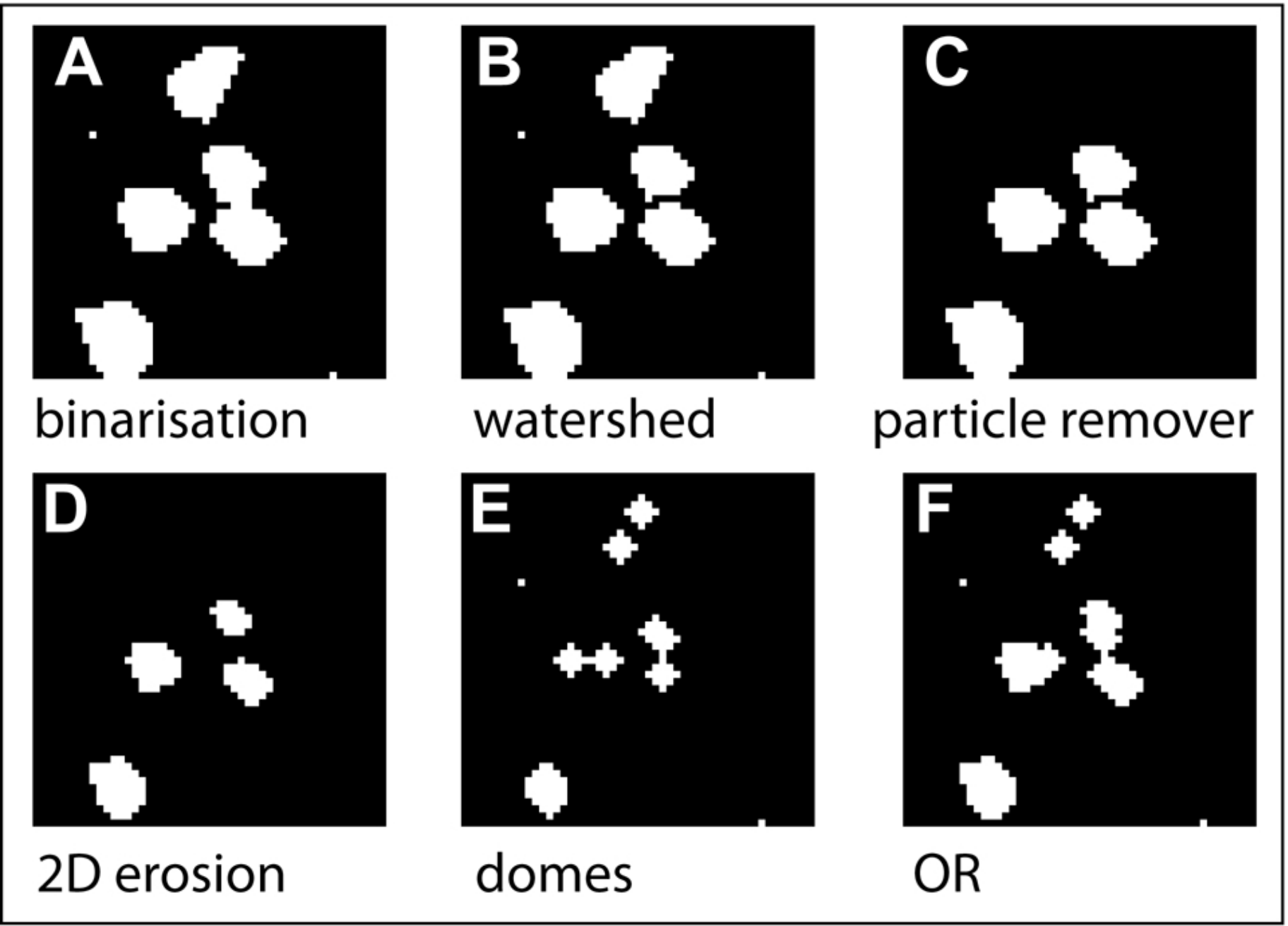

Figure 6 Images resulting from the process to solve the problem shown in Figure 5.

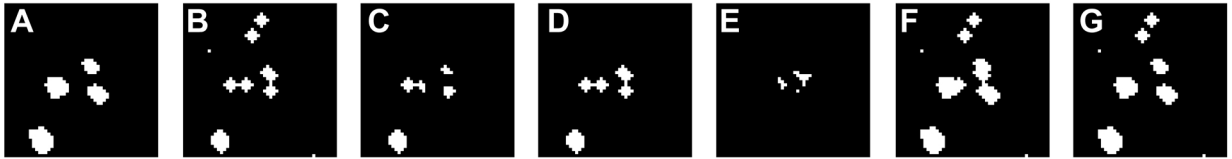

Figure 7 Automatic counting of manually selected glia

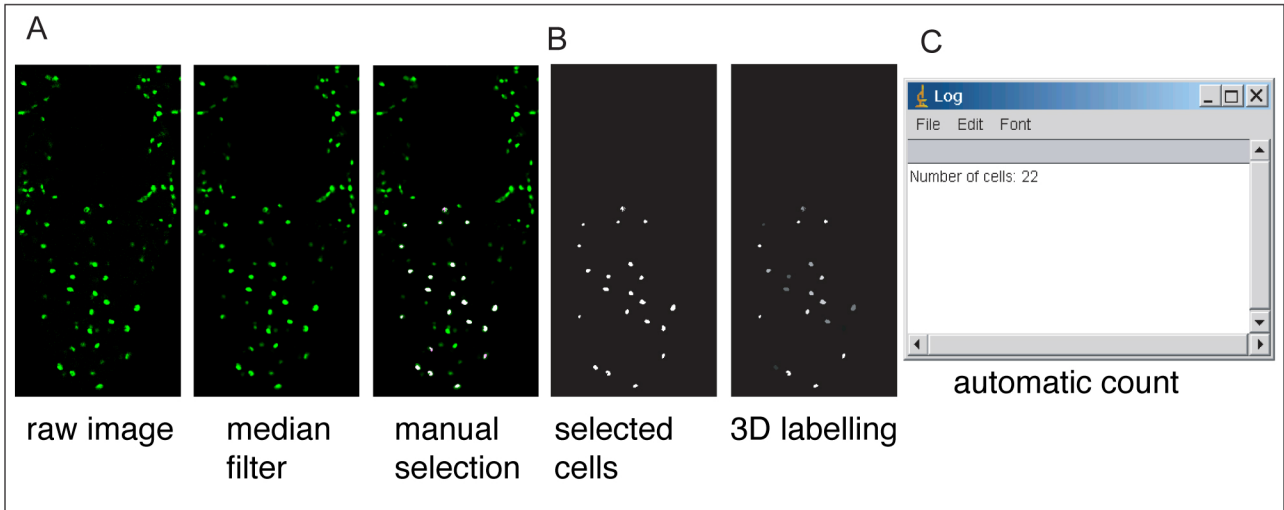

Figure 8 Validation and biological application

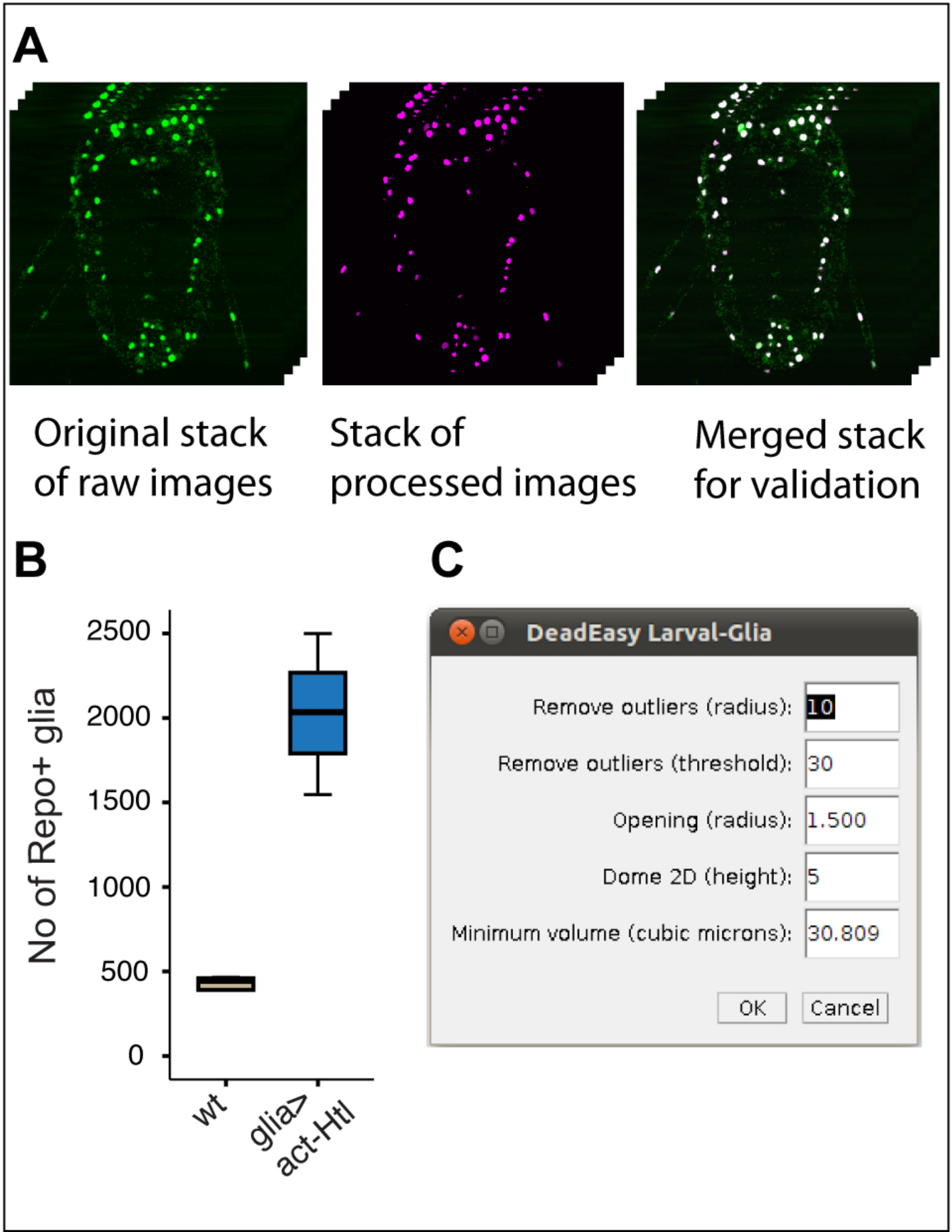

Figure 9

Cell separation by CellSegmentation 3D compared to DeadEasy

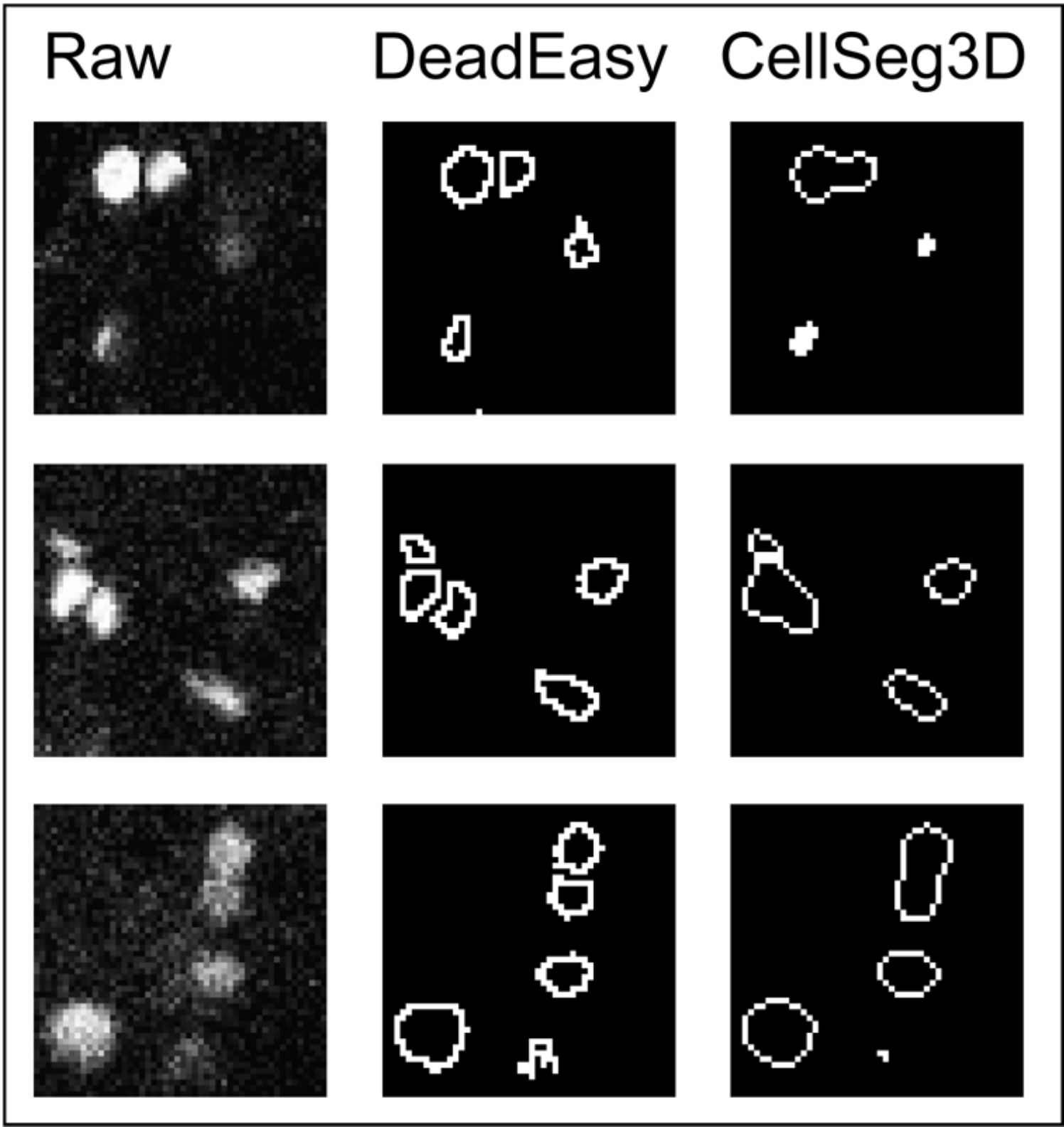

Figure 10 How well DeadEasy Larval Glia performs on other sample types

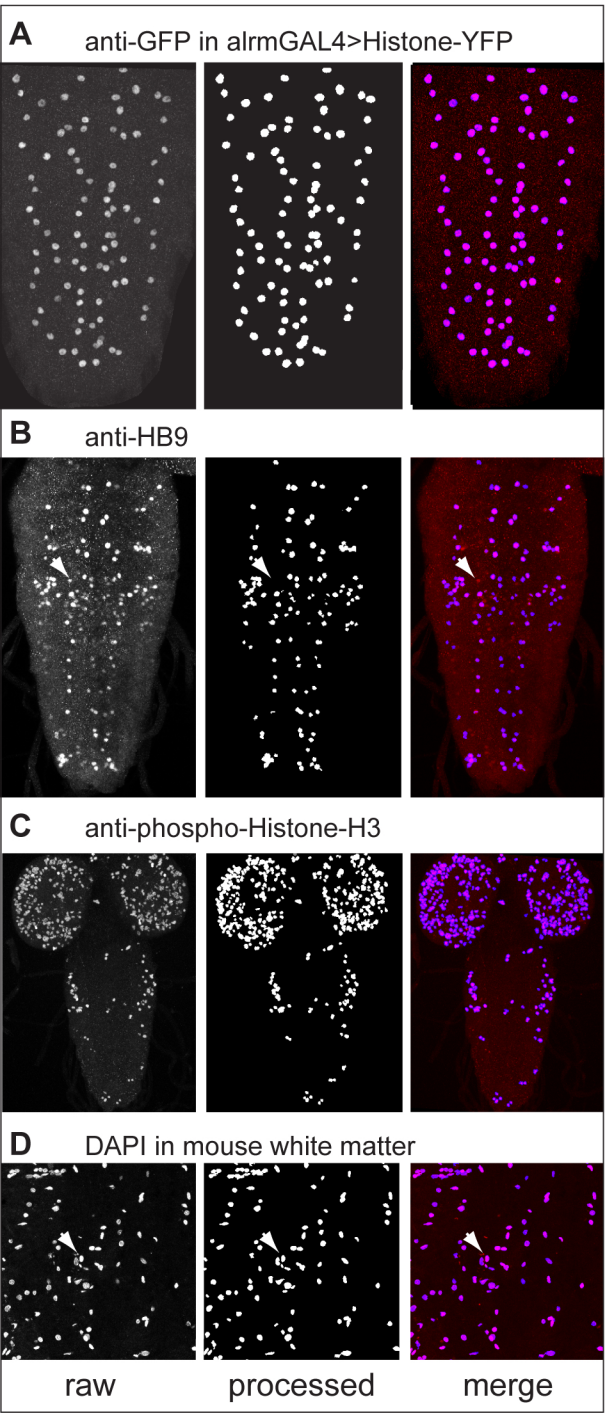

Table 1. Variation in the number of counted cells for different values of h.

	h								
STACK	**2**	**3**	**4**	**5**	**6**	**7**	**8**	**9**	**10**
1	85	85	85	85	85	84	84	84	84
2	125	124	123	121	120	120	120	119	119
3	122	121	121	121	121	121	121	119	119
4	82	81	81	81	81	81	81	81	81
5	116	114	112	111	110	110	109	109	109
6	65	64	64	63	62	62	62	62	61
7	58	58	58	58	58	58	58	57	57
8	90	90	89	88	88	87	87	87	87
9	115	115	115	115	115	115	115	115	114
10	74	74	74	74	74	72	71	72	72

Table 2. Statistical results of the analysis of compactness of clusters of cells.

	Compactness
Mean	0.62631868
Standard Deviation	0.11930354
Min	0.26
Max	0.85

Table 3 Validation

Sample	Real No	DeadEasy Result	FP	FN	DeadEasy x 3 mean	s.d.	A x 3 mean	A s.d.	ABC mean	ABC s.d.
1	87	85	0	2	85	0	78.67	6.35	84.00	8.19
2	134	118	0	16	118	0	108.00	14.80	118.67	20.50
3	123	121	0	2	121	0	108.33	3.06	114.33	9.02
4	81	81	0	0	81	0	82.33	4.93	81.67	2.31
5	112	111	0	1	111	0	99.00	5.20	108.00	13.75
6	65	61	0	4	61	0	61.00	2.65	63.00	5.00
7	59	58	0	1	58	0	58.33	0.58	57.33	1.15
8	89	83	0	6	83	0	84.67	3.51	89.67	2.08
9	118	115	0	3	115	0	111.67	2.89	114.33	6.66
10	79	74	1	6	74	0	71.33	3.06	74.00	4.00
Total	**947**	**907**	**1**	**41**	**90.7**	**0**	**86.33**	**4.70**	**90.50**	**7.27**
		%FP	0.11							
		%FN	4.33							

Real Number' is the number of cells counted after verifying each cell, one at a time, comparing the DeadEasy result with the raw image. 'DeadEasy Result' is the number of cells identified as such by the programme. FP: number of false positives; FN: number of false negatives. DeadEasy x 3 mean: DeadEasy results are identical regardless of the number of times counted (here three as an example). A,B,C are three different researchers: 'A x 3 mean' corresponds to three different scorings by A; 'ABC' is the pooling of the scores by A+B+C. s.d.: standard deviation.

Table 4
Compared performance of DeadEasy vs. CellSegmentation 3D

Method	Mean	% False (+)	% False (-)
DeadEasy LarvalGlia	91	0.1	4.32
CellSegmentation3D (min. 50)	86	0	12.77
CellSegmentation3D (min. 15)	88	0.74	8.02

Table 5. Parameters that can be altered and their effects.

DeadEasy Larval Glia: Parameters that can be altered and their effects	
Threshold	This is to separate signal from noise. Increasing the radius will increase the number of pixels considered to calculate the local threshold. A minimum threshold must be defined to prevent noise in darker areas.
Opening	This is to eliminate noise. Increasing the radius of the opening will remove more small particles, so the number of counts will decrease.
Dome 2D	This is optimal to detect objects (i.e. nuclei) that are tightly packed (i.e. the staining detects many of them) and with varying signal intensity. Increasing the height of the dome will reduce the number of objects given that local small domes will be combined in higher domes, and several cells will be detected as one.
Compactness	This it to detect circular and elliptical objects (e.g. nuclei). Increasing the minimum value of the compactness will reduce the number of detected objects, since only objects closest to being circular will be accepted.
Hu's third moment	This is to detect object symmetry. Decreasing the minimum value of this parameter will decrease the number of detected objects, since only the most symmetrical objects will be detected.
Volume	Increasing the minimum volume and decreasing the maximum volume will decrease the count, given that more particles will be excluded. For a different sample type, the minimum volume could be increased if the stained nuclei were larger than for our case.

This table shows on the left the parameters that the user can modify; on the right are summarised the consequences that modifying the parameters will have on object identification (i.e. cell counts). Indications are given on how the parameters could be modified if using different sample types (e.g. different tissues) or stainings. Any parameter modification will require cycles of validation and further modification by the user, until the desired accuracy for the sample and staining in use is reached.